Fabrication of radially aligned electrospun nanofibers in a three-dimensional conical shape

Research Article

Michel Vong and Norbert Radacsi*

Fabrication of radially aligned electrospun nanofibers in a three-dimensional conical shape

https://doi.org/10.1515/esp-2018-0001
Received March 08, 2018; accepted May 09, 2018

Abstract: This paper reports on the rapid fabrication of radially-aligned, three-dimensional conical structures by electrospinning. Three different polymers, Polyvinylpyrrolidone, Polystyrene and Polyacrylonitrile were used to electrospin the cones. These cone structures are spreading out from a vertical conductive pillar, which can be arbitrarily placed on specific part of the collector. The lower part of the cone is clearly defined on the collector, and the cone has a relatively uniform radius around the pillar. The cones are constituted of fibers that are radially aligned towards the top of the pillar, but there is no apex and the fibers fall flat on the top of the pillar surface. A parametric study has been performed to investigate the effects of the pillar morphology (height and thickness) and the electrospinning parameters (applied voltage and working distance) on the overall shape and size of the cone structure, as well as the fiber alignment. The pillar morphology influences directly the cone diameter and height. The electrospinning parameters have little effect on the cone structure. The formation mechanism has been identified to be related to the shape of the electric field, which has been systematically simulated to understand the effect of the electric field lines on the final dimensions of the cone structure.

Keywords: Electrospinning, Highly-stable, Cone, Radial alignment, 3D, Controlled shape, Conductive pillar

1 Introduction

Electrospinning is a simple technique that allows fabrication of micro- to nano-sized fibers from a polymer solution by applying a high voltage [1, 2]. Characteristics of electrospinning include high tunability over the fiber dimension and morphology, high versatility over the type of polymer that can be electrospun, and possible functionalization of the fibers [3–8]. This makes it a technique of choice for a wide range of applications, for example tissue engineering, drug delivery, filtration, catalyst support, sensors and energy devices [9–18].

While standard electrospinning gives rise to flat nonwoven fiber mats, several ways have been identified for inducing a preferential alignment to the fibers. However, the common fiber alignment methods either require precision fiber deposition by utilizing the stable jet part of electrospinning; mechanical movement with a high-speed rotating drum collector [19]; or manipulation of the electric field by adding insulating blocks on the pathway of the fibers [20]. Advantages of aligned fibers among others include guidance for growth for biological cells, or improved electrical and mechanical properties for energy devices [21–26]. Transition from a two-dimensional to a three-dimensional (3D) electrospun structure is therefore often desirable, as 3D electrospun structures can be beneficial as scaffolds for bio-engineering applications, or can serve as membranes for water splitting and filtration [27–30]. One way for achieving 3D electrospun structures is by extending the electrospinning time, and stacking several mats of fibers on top of each other [31]. The main issue of this technique is that the achievable height is low or each fiber layers are not interconnected to each other, preventing propagation of cells through the distinct layers [32, 33]. One way to circumvent this problem is to add one heating step to partly fuse the layers [34]. Other fabrication routes for 3D electrospun fibers are: electrospinning directly on a 3D auxiliary template, post-processing of the fibers, and direct self-assembly of the polymer fibers [35–38]. Examples of 3D auxiliary templates can include tubular collector or 3D printed scaffold [39, 40]. The obtained 3D structures do not possess any preferential alignment. Other ex-

***Corresponding Author: Norbert Radacsi:** Institute for Materials and Processes, School of Engineering, The University of Edinburgh, King's Buildings, Edinburgh, EH9 3FB, United Kingdom of Great Britain and Northern Ireland; Email: n.radacsi@ed.ac.uk
Michel Vong: Institute for Materials and Processes, School of Engineering, The University of Edinburgh, King's Buildings, Edinburgh, EH9 3FB, United Kingdom of Great Britain and Northern Ireland

amples include freeze drying of fibers mats or embedding the mats in hydrogel [41]. In both cases, it is possible to first electrospin aligned fibers mats before building the 3D structure [42, 43]. Overall, most of these techniques have the disadvantages of requiring long elaboration time or possessing poor control over the 3D structure. Combination of 3D printing with electrospinning can also be used to build different shapes for scaffolds within a short time, with a good control of the 3D shape, but fiber alignment has not been demonstrated so far [44].

In this paper, the fabrication of well-defined electrospun 3D cone structures with radial alignment is investigated. These cone structures were electrospun in a single step, onto the supportive material directly, which was a grounded conductive pillar. The influence of the pillar dimensions (height and thickness) on the morphology of the electrospun cone structures was studied systematically. Interactions between different cone structures in close proximity were observed as well. The effect of two electrospinning parameters (applied voltage and working distance) on the cone shape and size, and the structure of the fibers at different distances from the conductive pillar were also investigated. The alignment of the electrospun fibers was directly observed via Scanning Electron Microscopy (SEM) and the macroscopic architecture of the cone structures was studied by a digital mirror-reflex camera. The cone formation and radial alignment can be explained by analyzing the electric field in the vicinity of the grounded pillar. Radially aligned electrospun fibers have been reported to enhance and direct cell migration from the periphery to the center of the structure [45, 46]. The technology investigated in this paper combines the benefits of radially aligned fibers with 3D structures, and can be used as scaffolds for different applications [47].

2 Experimental

2.1 Materials

Polyvinylpyrrolidone (PVP, Mw=1,300,000), Polystyrene (PS, Mw=280,000), Polyacrylonitrile (PAN, Mw=150,000) were purchased from Alfa Aesar, Sigma Aldrich and Shandong Jianofu Treasure Industrial Co., respectively, and used without further purification. Filtered deionized water was used for dissolving PVP. Dimethylformamide (DMF) and tetrahydrofuran (THF) were acquired from Alfa Aesar and Fisher Scientific, respectively. The 0.3 mm and 0.7 mm thick graphite pillars were purchased from Staedtler, Germany. The 0.5 mm ones were obtained from Rotring, Germany. The 2 mm graphite pillar was acquired from Koh-i-Noor Hardtmuth, Austria. The 5.6 mm graphite pillar was received from e+m, Germany. Polyactic acid (PLA) filament was acquired from Ultimaker, Netherlands. The 1.1 mm thick steel/copper pillar was acquired from Office Depot, United Kingdom. The 0.3 mm thick aluminum support was acquired from Parthian Energy, USA.

2.2 Support construction

The collecting supports were designed using a Computer Aided Design (CAD) software (Onshape v1.75). The supports were circles with a radius of 4.0 cm, with holes to insert the graphite pillars. The PLA supports were 3D printed with an extrusion-based 3D printer (Ultimaker 3, Ultimaker, Netherlands), and wrapped in a conductive aluminum foil. The graphite pillars were cut to the desired height with a Stanley knife and inserted inside the PLA supports. The pillar height was controlled with an electronic digital caliper (500-196-30, Mitutoyo, Japan) with an accuracy of 0.1 mm. The shortest and thinnest pillar support (0.7 mm high and 0.3 mm thick) was made by carving an aluminum frame with a Computer Numerical Control mill. Overall, the support was a conductive pillar standing on a circular base.

2.3 Electrospinning apparatus and procedure

The electrospinning apparatus (NovaSpider, CIC nanoGUNE, Spain) consists of a syringe pump, connected to a nozzle head through a polytetrafluoroethylene (PTFE) tube. The high voltage was applied directly to the nozzle head. The device is capable of moving the nozzle head in the x-y plan, with a resolution of 0.02 mm, to spread the fibers deposition over a wide area. The collector bed height can be set along the z axis. Figure 1 depicts an illustration of the 3D electrospinner as well as the experimental setup with pillar support.

15 wt% PVP was dissolved in water at room temperature for 5 hours. 15 wt% PAN and 15 wt% PS were dissolved in pure DMF and 1:1 DMF/THF respectively. The solution was loaded into a syringe connected to a blunt needle (nozzle) through the PTFE tube. The applied voltage to the nozzle was set between 8 and 20 kV, the flow rate was fixed to 0.25 $mL.h^{-1}$, the working distance was varied between 5 and 20 cm, and the needle gauge was 22G (inner diameter = 0.413 mm). The pillar support was placed in the center of the grounded collector, which was beneath the

Table 1: Summary of all electrospinning conditions. The parameters kept at a constant value during the parametric study are highlighted.

Constant parameters	**15 wt% PVP/H_2O - Flow rate 0.25 mL·h^{-1} - Needle 22G**		
Pillar height (mm)	Pillar thickness (mm)	Applied voltage (kV)	Working distance (cm)
1	0.3	8	5
2	0.5	14	10
3	0.7	20	15
4	0.9		20
5	2.0		
7.5	5.5		
10			

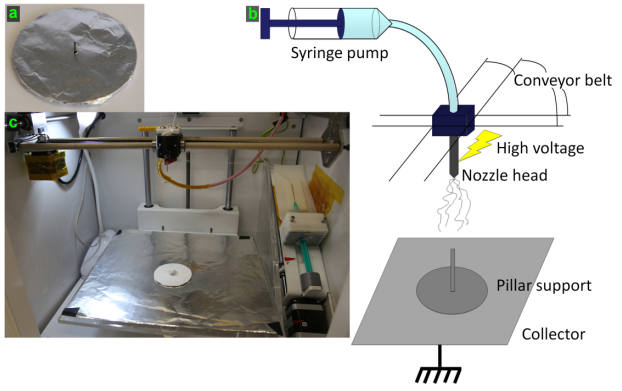

Figure 1: (a) Close-up photo of a typical pillar support without the electrospun fibers. **(b)** Schematic drawing of the experimental setup with pillar support. **(c)** Picture of the electrospinning chamber with the electrospun sample in the center.

nozzle head. The nozzle head was moving in a 4.9 cm*3.2 cm area to spread the fibers onto the whole pillar support. The experiments were carried out for 10 minutes at room temperature, between 20-27°C, with the relative humidity between 45-50%, as measured by a temperature and humidity sensor (HumidiProbe, Pico Technology, United Kingdom).

The cone shapes have been measured by direct observation of their macroscopic features with a digital camera. The effect of the process parameters (pillar height, pillar thickness, applied voltage and working distance) over the shape of the cone structure has been investigated. This was done with a parametric study where only one parameter at a time would be changed between each experiment. The different experimental conditions (pillar size and electrospinning conditions) are summarized in Table 1.

2.4 Characterization

The macroscopic shape of the cone structure was captured using a digital camera (EOS 6D, Canon Inc., Japan). The microscopic structure and the alignment of the fibers were observed with a Scanning Electron Microscope (SEM) (JSM-6010PLUS/LV, JEOL Ltd., Japan) at an accelerating voltage of +20 kV. The cone diameters were measured using an image processing software (Fiji - ImageJ v1.51u). The fiber alignment was characterized using the plug-in 'Directionality' (v2.0.2) included in the Fiji software. The Fast Fourier Transform (FFT) of the picture was analyzed and converted into a histogram depicting the number of fibers at every 2 degrees between 0 to 180°. 0° is the East direction and the angle goes up in a counterclockwise trend. The samples were coated with 20 nm of Gold using a Sputter Coater (Desk III, Denton Vacuum, USA) before observation.

2.5 Electric field simulation

The electric field simulations were performed with a finite element analysis software, solver and multiphysics simulation software (COMSOL Multiphysics – v5.3a). The syringe needle was defined as a steel hollow cylinder with an outer diameter of 0.8192 mm, an inner diameter of 0.5140 mm and a height of 2 cm. The collector was an aluminium rectangle with a length of 26 cm, a width of 20 cm and a thickness of 0.5 cm. The pillar support was drawn as an aluminum circular base with a diameter of 4 cm and a thickness of 0.5 cm. The dimensions of the graphite pillar, the working distance and the applied voltage to the needle were adjusted accordingly to the experimental parameters. The boundary domain was defined as a rectangular box with a length of 31 cm, a depth of 25 cm and a height 5 cm higher than the working distance of study. The mesh

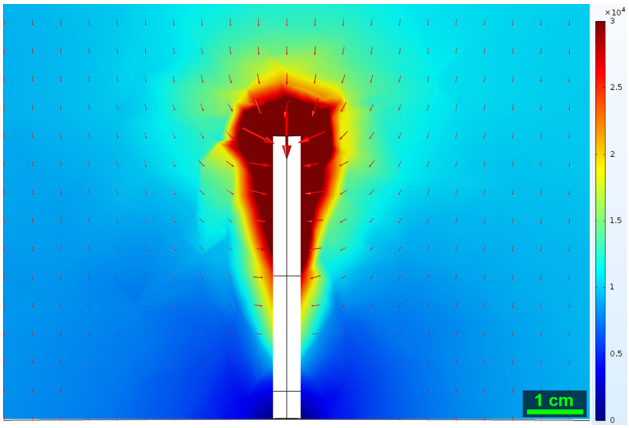

Figure 2: Electric field simulation in the vicinity of the grounded pillar. The electric field is the highest at the top of the pillar and is pointing to it. The electric field scale is in $V \cdot m^{-1}$.

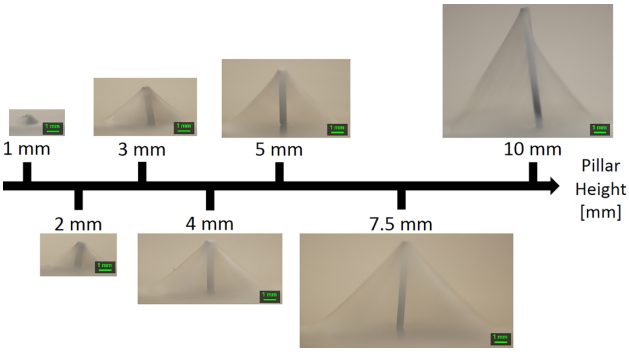

Figure 3: Evolution of the cone morphology as the pillar height is increased from 1 mm to 10 mm. The overall cone shape is still observed at the pillar height of 10 mm. The pillar thickness was fixed at 0.5 mm.

was set to a "Fine" size. The electric field was examined in the y-z plane, in the vicinity of the grounded pillar.

3 Results and discussion

3.1 Cone shape

The formation of the aligned cone-shaped electrospun fibers is driven by the electric field. Due to the presence of the conductive pillar in the center, the electric field lines are concentrated to the top of the pillar, where the electric field is the highest (Figure 2) [48]. During the elecrospinning process, the emitted charged fibers from the nozzle are attracted towards the top of the grounded pillar. As soon as a charged fiber touches the grounded pillar, the charges at the front end are neutralized. However, the part of the electrospun fibers far enough from the grounded pillar is still positively charged because of the low electrical conductivity of the polymer fiber. That positively charged part is still influenced by the electric field, until it touches the flat part of the collector. The shape of the electric field, and thus the shape of the electrospun truncated cone structure, is heavily influenced by the pillar morphology itself. A similar formation mechanism of an electrospun cone structure was described by Zhou *et al.* [49].

The top part of the cone was spreading out from the tip of the conductive pillar. The cone structures could not be clearly defined with an apex. The top of the cone structure was flat, as the fibers were strongly attracted by the grounded pillar. The flat base of the polymer cone had an irregular circle shape. This was most likely due to the imperfections of the graphite pillar, being dented after cutting them to size. These defects were minimal, with the radiuses along the circle having a deviation lower than 10% in most cases.

The shape of the pillars has a direct influence on the height of the cone structure, as well as its diameter. As seen in Figure 3, the pillar height is the parameter that has the most influence on the cone dimensions. This is because the shape of the electric field in the vicinity of the pillar is directly affected by the height of the pillar, the position of the top of the pillar to the grounded collector. An example of electric field simulation is shown in Figure 2. The electric field simulation for the other pillar heights are shown in the Supplementary S1. Similar to the setup designed by Zhou *et al.*, the electric field is oriented toward the top of the pillar. Moving further away from the tip of the grounded pillar to the flat collector, the electric field slowly reorients to a vertical direction. As such, increasing the pillar height alters directly the electric field in the vicinity of the pillar. With a higher pillar, the electric field lines are influenced and redirected on a longer distance, both on the horizontal and the vertical axis. This results in an increased cone diameter with higher pillars as the distorted electric field influences the travel path of the electrospun fibers. The measured mean cone diameters were 2.5 ± 0.1, 5.4 ± 0.2, 7.6 ± 0.1, 10.2 ± 0.1, 10.0 ± 0.2, 15.3 ± 0.1, 13.9 ± 1.0 mm for the pillar height from 1 to 10 mm respectively (see Figure 4). The cone structure electrospun with the 10 mm pillar is the one deviating the most from the growing trend. This is due to the pillar itself leaning to the side and preventing the formation of the cone structure from the top of the pillar. It was not possible to see if there was a minimum pillar height at which no more cone structures would be electrospun due to limitation in cutting method. Yang *et al.* could still observe a cone structure with a pillar height of 0.1 mm and a thickness of about 0.5 mm [50]. The increasing trend of the cone diameter with the pillar height from

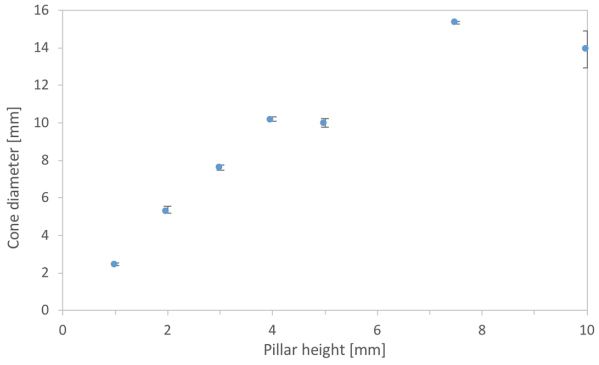

Figure 4: Evolution of the cone diameter as the pillar height is increased from 1 mm to 10 mm. The cone diameter increases with the pillar height except for the pillar heights of 5 and 10 mm. The pillar thickness was 0.5 mm.

0.1 mm to 0.7 mm was still followed as well in their work. It was noted, however, that the maximum pillar height is mostly limited by the close proximity between the top of the pillar and the charged nozzle. This can either induce a short circuit because of the high voltage, an unstable electrospinning process or improper drying of the electrospun jet. All these reasons can prevent the proper formation of the cone structure.

At first glance (see Figure 5), the pillar thickness seems to have an effect on the cone diameter (measured at its base), increasing linearly with it, except for the 5 and 10 mm pillar heights. The measured cone diameters were 10.7 ± 0.1, 10.0 ± 0.2, 11.2 ± 0.1, 11.3 ± 0.2, 12.8 ± 0.3, 15.7 ± 0.2 mm for the pillar thickness 0.3, 0.5, 0.7, 0.9, 2.0 and 5.5 mm respectively (see Figure 6). It is however observed that, when taking into account the size of the conductive pillar itself, the actual cone diameter stays at about 10 mm independently from the pillar thickness. This implies that the electric field lines at the sides of the conductive pillar do not change with the pillar thickness, thus the low influence on the fiber travel path, and the cone diameter. This observation is shown in Supplementary S2. These simulations show the behavior of the electric field lines, at the side of the pillar, is independent of the pillar thickness. Regardless of the pillar thickness, only the electric field lines located within 2-3 cm at the side of the grounded pillars are diverted and reoriented.

A number of applied voltages and working distances have been tested to investigate the influence of the electrospinning parameters. The pillar height was fixed at 5 mm and the thickness was at 0.5 mm. As seen in Figure 7 and Figure 8, these electrospinning parameters have little to no influence on the macroscopic shape of the cone structure. This is because these two parameters, in this range of study, do not alter the shape of the electric field around the conductive pillar, and the travel path from the top of the

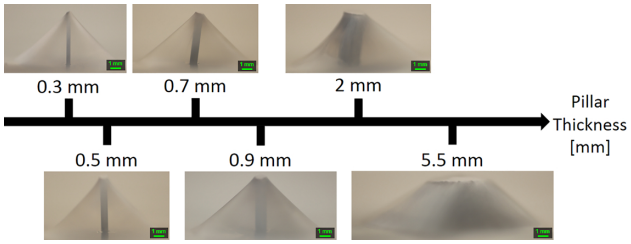

Figure 5: Evolution of the cone morphology as the pillar thickness is increased from 0.3 mm to 5.5 mm. The cone gets larger as the pillar thickness increases. The pillar thickness was 0.5 mm.

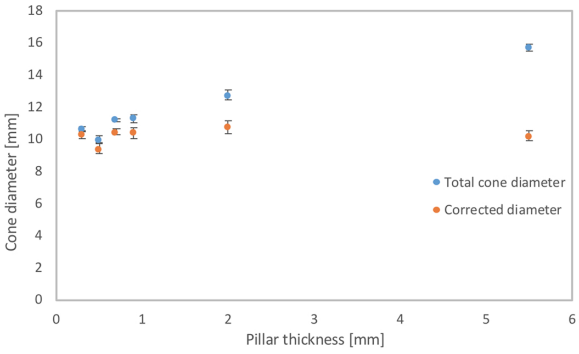

Figure 6: Evolution of the cone diameter as the pillar thickness is increased from 0.3 mm to 5.5 mm. The corrected diameter (cone diameter at the base minus the pillar thickness) stays relatively constant with the pillar thickness. The pillar height was kept at 5 mm.

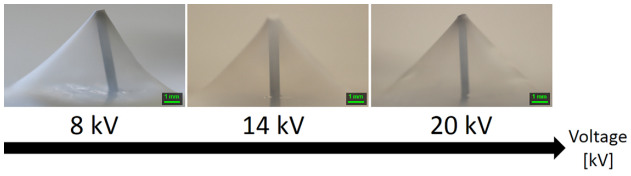

Figure 7: Evolution of the cone morphology as the voltage is increased from 8 to 20 kV. The cone morphology does not change in this range of voltage. The pillar height was 5 mm and the thickness was 0.5 mm.

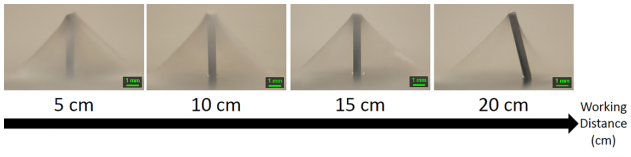

Figure 8: Evolution of the cone morphology as the working distance is increased from 5 to 20 cm. The cone morphology does not change with the working distance. The pillar height was 5 mm and the thickness was 0.5 mm.

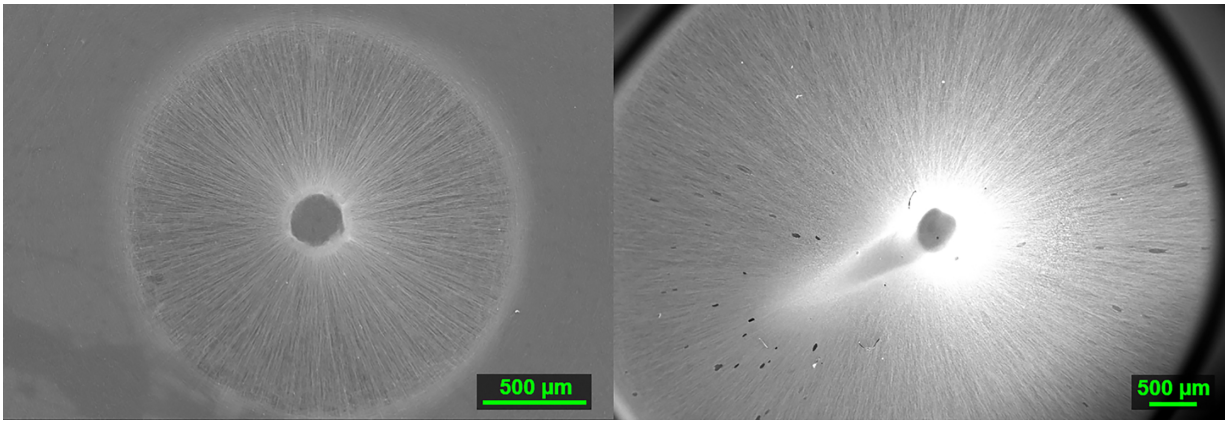

Figure 9: Top-view of the pillar support after electrospinning. The cone shape as well as the alignment of the fibers toward the top of the pillar is observable. **Left:** Pillar height 0.7 mm and thickness 0.3 mm. **Right:** Pillar height 5 mm and thickness 0.3 mm.

pillar to the grounded collector remains unchanged. This is highlighted in the electric field simulation of the Supplementary S3 and Supplementary S4, where the direction and orientation of the electric field are independent from the applied voltage and the working distance. Because of the grounded pillar, these 2 parameters only influence the electric field intensity rather than the electric field lines. This also implies that the electric field intensity by itself has no influence on the shape of the electrospun cones. As a result, all the cones electrospun at different voltages and working distances have diameters of about 1.0 mm. It was, however, worth noting that the cones electrospun at a working distance of 20 cm had less fibers than the other cones. This is mostly due to the configuration of the electrospinning device itself and, at this working distance, some fibers are diverted from the grounded collector, thus resulting in a fewer amount of fibers.

3.2 Fiber alignment

SEM images have been taken for different pillar thicknesses, from 0.3 mm to 2.0 mm, as well as two different pillar heights, 0.7 mm and 5.0 mm. Similar fiber alignment was seen with all the pillar dimensions (see Supplementary S5).

As shown in Figure 9, there is a general alignment of the fibers towards the top center of the pillar support. By zooming in at the edge of the pillar support, as seen in Figure 10, it is observed that the fibers deposited on top of the pillar are randomly oriented, and they get their relative radial orientation towards the center of the pillar only when they leave the pillar. This behavior is independent from the pillar thickness. Analysis performed by the Directionality plugin of the Fiji software showed that the fibers are well-aligned with an average standard deviation below 10°, independently from the thickness or height of the pillars (see Supplementary S5). The flat top pillar, on a microscopic level, acts as a regular flat collector and cannot induce any preferential orientation. This alignment behavior is similar to the work done by Xie *et al.*, where a point electrode was used in the middle of a ring electrode to induce a radial alignment [45]. They simulated the electric field to show that it was pointing to both the point and the ring electrode, thus favoring the radial alignment.

The other edge of the cone, where the fibers touch the flat part of the collector, was also investigated by SEM. There was no transition zone present, as seen in Figure 11. The fibers suddenly lost any radial orientation and the clear frontier of the cone was observed. This observation could be mostly attributed to the fact that the images were taken from a top view, so only the upper layer of the fibers was observed. If there was any other unoriented layers underneath, they would be hidden by the top layer. The fibers deposited far away from the pillar support are randomly oriented. This is because away from the pillar, the electric field and the behavior of the electrospun fibers are similar to conventional electrospinning onto a flat grounded collector.

Finally, it has been observed that the distance between two pillars can affect the cone formation. When the pillars are in close proximity, the fibers would form a linear network and connect the two pillars together (bridging effect), as seen in Figure 12. A similar phenomenon has been observed by Pan *et al.*, although they placed an insulating layer on top of the conductive support [51]. This prevented the formation of any cone structure and they focused their work on the fiber network within the array of pillars. This linear network has also been observed with insulating pillar support [52–54]. Our hypothesis is that this bridging ef-

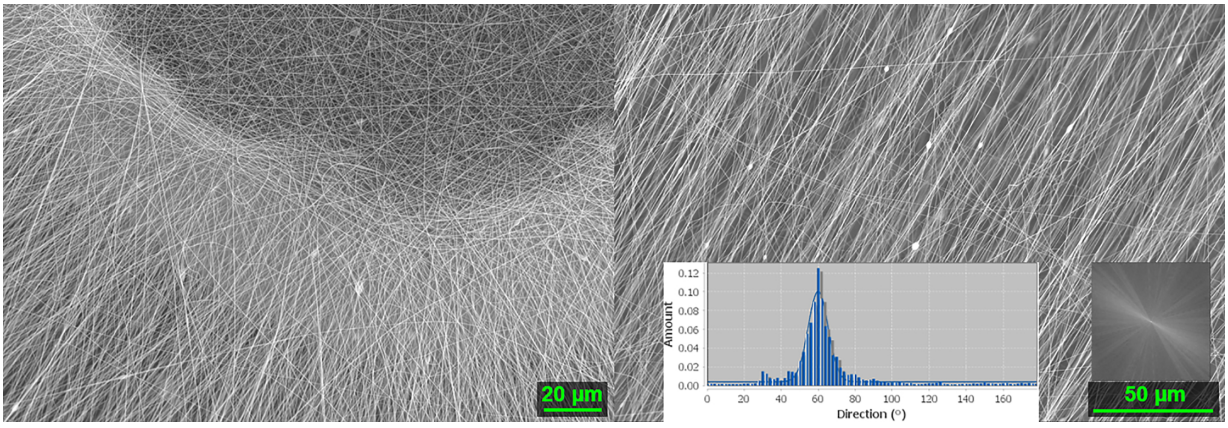

Figure 10: SEM picture of the pillar support after electrospinning. **Left:** Zoom-in at the edge of the central pillar. **Right:** Zoom-in of the aligned fibers hanging from the top of the pillar with its associated FFT and fibers orientation histogram. The pillar itself had a height of 5 mm and a thickness of 0.3 mm. The alignment of the fibers on specific part of the cone is observable.

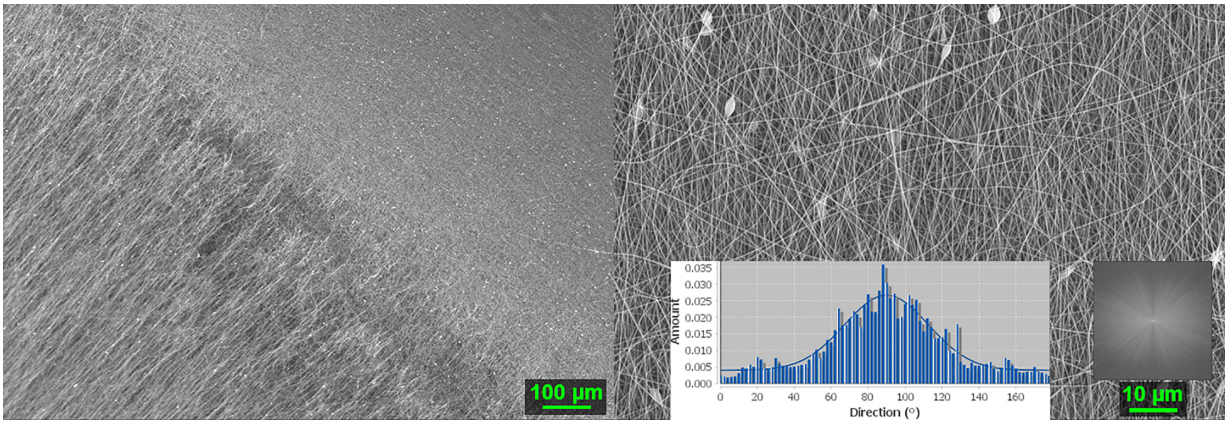

Figure 11: SEM picture of the surrounding of the pillar (height 5 mm and thickness 0.3 mm) after electrospinning. **Left:** Outer edge of the cone. **Right:** Far away from the pillar and the cone with its associated Fast Fourier Transform and fiber orientation histogram. The random alignment of the fibers far away from the pillar is observable.

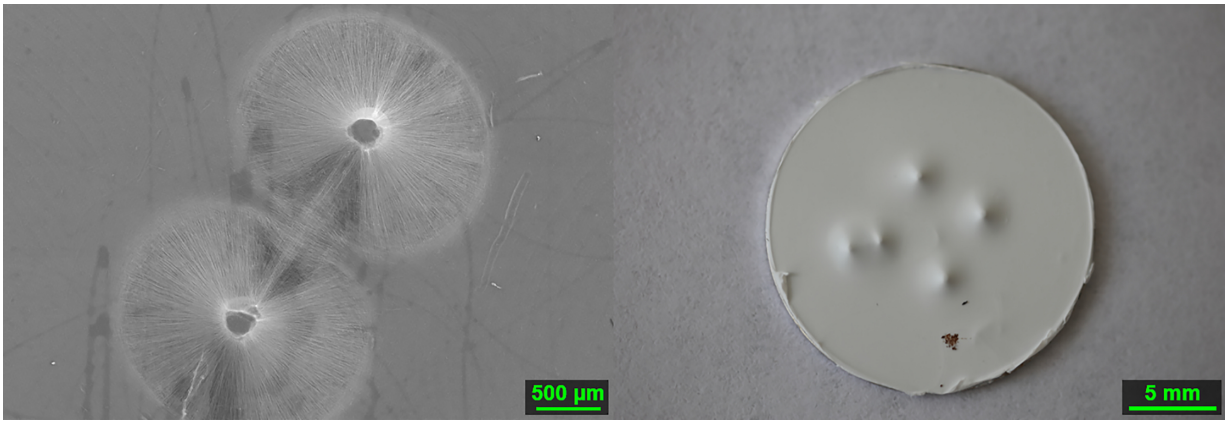

Figure 12: Left: SEM picture after electrospinning of a support containing two pillars in close proximity. Two 0.7 mm high and 0.3 mm thick pillars separated by a distance of 1.4 mm. A linear fiber network (bridging) between pillars is observable at this distance. **Right:** Photograph of a support containing multiple pillars. The 2 pillars on the left are separated by a distance of 1.4 mm. The other pillars have a distance of 4.0 mm between them. Interactions between cones are observed when the conductive pillars are close to each other.

fect would happen when the distance between the two pillars is inferior to the sum of the radius of the two cones, as the fibers of the cones would be able to interact with each other. As shown in Figure 12, even when putting multiple pillars over the same support, there is little to no distortion of the cone structure when the pillars are distant enough from each other.

3.3 Extension to other polymers and pillar materials

The fabrication of cone structures using electrospinning has been achieved with the polymers PAN and PS as well. The diameter of the electrospun cones were of 11.4 ± 0.2 and 16.9 ± 0.1 mm for PAN and PS respectively. The process parameters at which these cones were formed are highlighted in Table 1. Both of these diameters are larger than the cone diameter obtained with PVP (10 ± 0.2 mm) under the same experimental conditions. The higher resistivity of the PS polymer compared to the PVP and PAN might be directly correlated to the larger cone structure [55–57]. More electric charges are retained by the PS fibers, which makes them more susceptible to the sudden change of electric field next to the grounded pillar [58]. This results in a larger cone structure. The electrospun PAN and PS cones also feature radial alignment toward the top of the grounded pillar. In addition, the fabrication of the cone structure on a different pillar material has been achieved as well. A cone diameter of 13.4 ± 0.1 mm was obtained for a steel/copper pillar.

These additional cone structures are illustrated in Supplementary S6.

3.4 Conclusions

This work reports on the fast and facile electrospinning of aligned 3D cone structures, using conductive pillars sticking out of the grounded collector. These cone structures are electrospun within 10 minutes and highly stable, even after 6 months of storage at ambient conditions. The cones are constituted of radially-aligned fibers toward the top of the cones, attached to a vertical and conductive pillar that is connected to the ground. The base of the electrospun cones is a rather uniform circle around the conductive pillar. The fibers on top of the conductive pillars and the fibers far away from the pillars show a random orientation as the electric field is not affected by the pillar at those places. The effect of the electrospinning parameters and pillar dimension on the cone morphology, and the formation mechanism have been investigated. The cone structure is formed due to the distorted electric field in the vicinity of the conductive pillar, as well as the slow charge neutralization of the polymer fibers. The morphology of the cone structure is mostly dependent on the dimensions of the pillar itself, in particular the pillar height. The electrospinning parameters have little to no influence on the cone structure as they do not alter the electric field itself. The electric field has been systematically simulated and show how the electric field lines directly interfere with the shape of the electrospun cone. The formation of a linear fibrous network between two pillars is observed when the pillars are in close proximity. It is suggested that these peculiar radially-aligned cone structures have potential applications in bio-engineering and sensors.

Acknowledgement: The SEM results were obtained using the EPSRC Centre for Doctoral training in "Soft Matter and Functional Interfaces" SEM. The authors would like to thank Jing Shan for her help in the English revision.

References

[1] Xue J, Xie J, Liu W, Xia Y, Electrospun Nanofibers: New Concepts, Materials, and Applications, Acc Chem Res. 50, 2017, 1976.
[2] Thenmozhi S, Dharmaraj N, Kadirvelu K, Kim HY, Electrospun nanofibers: New generation materials for advanced applications, Mater Sci Eng B. 217, 2017, 36.
[3] Jian S, Zhu J, Jiang S, Chen S, Fang H, Song Y, *et al.*, Nanofibers with diameter below one nanometer from electrospinning, RSC Adv. 8, 2018, 4794.
[4] Katsogiannis KAG, Vladisavljević GT, Georgiadou S, Porous electrospun polycaprolactone (PCL) fibres by phase separation, Eur Polym J. 69, 2015, 284.
[5] Huang Z-X, Wu J-W, Wong S-C, Qu J-P, Srivatsan TS, The technique of electrospinning for manufacturing core-shell nanofibers, Mater Manuf Process. 33, 2018, 202.
[6] Feltz KP, Kalaf EAG, Chen C, Martin RS, Sell SA, A review of electrospinning manipulation techniques to direct fiber deposition and maximize pore size, Electrospinning. 1, 2017, 46.
[7] Al-Ajrah S, Lafdi K, Liu Y, Le Coustumer P, Fabrication of ceramic nanofibers using polydimethylsiloxane and polyacrylonitrile polymer blends, J Appl Polym Sci. 135, 2018, 45967.
[8] Chen C, Tang Y, Vlahovic B, Yan F, Electrospun Polymer Nanofibers Decorated with Noble Metal Nanoparticles for Chemical Sensing, Nanoscale Res Lett. 12, 2017, 451.
[9] Zhang C, Wang X, Zhang E, Yang L, Yuan H, Tu W, *et al.*, An epigenetic bioactive composite scaffold with well-aligned nanofibers for functional tendon tissue engineering, Acta Biomater. 66, 2018, 141.
[10] Pedersbaek D, Frantzen MT, Fojan P, Electrospinning of Core-Shell Fibers for Drug Release Systems, J Self-Assembly Mol Electron. 5, 2017, 17.

[11] Alavarse AC, de Oliveira Silva FW, Colque JT, da Silva VM, Prieto T, Venancio EC, *et al.*, Tetracycline hydrochloride-loaded electrospun nanofibers mats based on PVA and chitosan for wound dressing, Mater Sci Eng C. 77, 2017, 271.

[12] Chou S-F, Woodrow KA, Relationships between mechanical properties and drug release from electrospun fibers of PCL and PLGA blends, J Mech Behav Biomed Mater. 65, 2017, 724.

[13] Jing L, Shim K, Toe CY, Fang T, Zhao C, Amal R, *et al.*, Electrospun Polyacrylonitrile–Ionic Liquid Nanofibers for Superior PM 2.5 Capture Capacity, ACS Appl Mater Interfaces. 8, 2016, 7030.

[14] Yousef A, Brooks RM, El-Halwany MM, Abutaleb A, El-Newehy MH, Al-Deyab SS, *et al.*, Electrospun CoCr 7 C 3 -supported C nanofibers: Effective, durable, and chemically stable catalyst for H 2 gas generation from ammonia borane, Mol Catal. 434, 2017, 32.

[15] Yang X, Li X, Zhang L, Gong J, Electrospun template directed molecularly imprinted nanofibers incorporated with BiOI nanoflake arrays as photoactive electrode for photoelectrochemical detection of triphenyl phosphate, Biosens Bioelectron. 92, 2017, 61.

[16] Mercante LA, Pavinatto A, Iwaki LEO, Scagion VP, Zucolotto V, Oliveira ON, *et al.*, Electrospun Polyamide 6/Poly(allylamine hydrochloride) Nanofibers Functionalized with Carbon Nanotubes for Electrochemical Detection of Dopamine, ACS Appl Mater Interfaces. 7, 2015, 4784.

[17] Jindal A, Narayanan H, Basu S, Direct Formic Acid PEM Fuel Cell with Electrospun Carbon Nitride Nanofibers as Cathode Catalyst, Fuel Cells. 17, 2017, 407.

[18] Hong S, Hou M, Zhang H, Jiang Y, Shao Z, Yi B, A high-performance PEM fuel cell with ultralow platinum electrode via electrospinning and underpotential deposition, Electrochim Acta. 245, 2017, 403.

[19] Yu L, Shao Z, Xu L, Wang M, High Throughput Preparation of Aligned Nanofibers Using an Improved Bubble-Electrospinning, Polymers (Basel). 9, 2017, 658.

[20] Hwang W, Pang C, Chae H, Fabrication of aligned nanofibers by electric-field-controlled electrospinning: insulating-block method, Nanotechnology. 27, 2016, 435301.

[21] Xie J, MacEwan MR, Liu W, Jesuraj N, Li X, Hunter D, *et al.*, Nerve Guidance Conduits Based on Double-Layered Scaffolds of Electrospun Nanofibers for Repairing the Peripheral Nervous System, ACS Appl Mater Interfaces. 6, 2014, 9472.

[22] Tamura T, Kawakami H, Aligned Electrospun Nanofiber Composite Membranes for Fuel Cell Electrolytes, Nano Lett. 10, 2010, 1324.

[23] Zhu J, Chen L, Xu Z, Lu B, Electrospinning preparation of ultralong aligned nanofibers thin films for high performance fully flexible lithium-ion batteries, Nano Energy. 12, 2015, 339.

[24] Sadrjahani M, Gharehaghaji AA, Javanbakht M, Aligned electrospun sulfonated polyetheretherketone nanofiber based proton exchange membranes for fuel cell applications, Polym Eng Sci. 57, 2017, 789.

[25] Pauly HM, Kelly DJ, Popat KC, Trujillo NA, Dunne NJ, McCarthy HO, *et al.*, Mechanical properties and cellular response of novel electrospun nanofibers for ligament tissue engineering: Effects of orientation and geometry, J Mech Behav Biomed Mater. 61, 2016, 258.

[26] Fee T, Downs C, Eberhardt A, Zhou Y, Berry J, Image-based quantification of fiber alignment within electrospun tissue engineering scaffolds is related to mechanical anisotropy, J Biomed Mater Res Part A. 104, 2016, 1680.

[27] Mellor LF, Huebner P, Cai S, Mohiti-Asli M, Taylor MA, Spang J, et al., Fabrication and Evaluation of Electrospun, 3D-Bioplotted, and Combination of Electrospun/3D-Bioplotted Scaffolds for Tissue Engineering Applications, Biomed Res Int. 2017, 2017, 1.

[28] Shen C, Wycisk R, Pintauro PN, High performance electrospun bipolar membrane with a 3D junction, Energy Environ Sci. 10, 2017, 1435.

[29] Matulevicius J, Kliucininkas L, Martuzevicius D, Krugly E, Tichonovas M, Baltrusaitis J, Design and Characterization of Electrospun Polyamide Nanofiber Media for Air Filtration Applications, J Nanomater. 2014, 2014, 1.

[30] Zhang Q, Welch J, Park H, Wu C-Y, Sigmund W, Marijnissen JCM, Improvement in nanofiber filtration by multiple thin layers of nanofiber mats, J Aerosol Sci. 41, 2010, 230.

[31] Soliman S, Pagliari S, Rinaldi A, Forte G, Fiaccavento R, Pagliari F, *et al.*, Multiscale three-dimensional scaffolds for soft tissue engineering via multimodal electrospinning, Acta Biomater. 6, 2010, 1227.

[32] Tzezana R, Zussman E, Levenberg S, A Layered Ultra-Porous Scaffold for Tissue Engineering, Created via a Hydrospinning Method, Tissue Eng Part C Methods. 14, 2008, 281.

[33] Pham QP, Sharma U, Mikos AG, Electrospun Poly(ε-caprolactone) Microfiber and Multilayer Nanofiber/Microfiber Scaffolds: Characterization of Scaffolds and Measurement of Cellular Infiltration, Biomacromolecules. 7, 2006, 2796.

[34] Cai Y-Z, Zhang G-R, Wang L-L, Jiang Y-Z, Ouyang H-W, Zou X-H, Novel biodegradable three-dimensional macroporous scaffold using aligned electrospun nanofibrous yarns for bone tissue engineering, J Biomed Mater Res Part A. 100A, 2012, 1187.

[35] Kim MS, Son J, Lee H, Hwang H, Choi CH, Kim G, Highly porous 3D nanofibrous scaffolds processed with an electrospinning/laser process, Curr Appl Phys. 14, 2014, 1.

[36] Moazeni N, Semnani D, Rafeinia M, Hasani H, Naeimi M, Sadrjahani M, The effect of electrospinning parameters on the compliance behavior of electrospun polyurethane tube for artificial common bile duct, Polym Sci Ser A. 59, 2017, 67.

[37] Mi H-Y, Jing X, Napiwocki BN, Li Z-T, Turng L-S, Huang H-X, Fabrication of fibrous silica sponges by self-assembly electrospinning and their application in tissue engineering for three-dimensional tissue regeneration, Chem Eng J. 331, 2018, 652.

[38] Sun B, Long YZ, Zhang HD, Li MM, Duvail JL, Jiang XY, *et al.*, Advances in three-dimensional nanofibrous macrostructures via electrospinning, Prog Polym Sci. 39, 2014, 862.

[39] Daming Z, Jiang C, Electrospinning of three-dimensional nanofibrous tubes with controllable architectures, Nano Lett. 8, 2008, 3283.

[40] Ostrowska B, Jaroszewicz J, Zaczynska E, Tomaszewski W, Swieszkowski W, Kurzydlowski KJ, Evaluation of 3D hybrid microfiber/nanofiber scaffolds for bone tissue engineering, Bull Polish Acad Sci Tech Sci. 62, 2014, 551.

[41] Domalik-Pyzik P, Morawska-Chochół A, Chłopek J, Rajzer I, Wrona A, Menaszek E, *et al.*, Polylactide/polycaprolactone asymmetric membranes for guided bone regeneration, E-Polymers. 16, 2016, 351.

[42] Lowe CJ, Reucroft IM, Grota MC, Shreiber DI, Production of Highly Aligned Collagen Scaffolds by Freeze-drying of Self-assembled, Fibrillar Collagen Gels, ACS Biomater Sci Eng. 2, 2016, 643.

[43] McMurtrey RJ, Patterned and functionalized nanofiber scaffolds in three-dimensional hydrogel constructs enhance neurite outgrowth and directional control, J Neural Eng. 11, 2014, 66009.
[44] Vong M, Speirs E, Klomkliang C, Akinwumi I, Nuansing W, Radacsi N, Controlled three-dimensional polystyrene micro- and nano-structures fabricated by three-dimensional electrospinning, RSC Adv. 8, 2018, 15501.
[45] Xie J, MacEwan MR, Ray WZ, Liu W, Siewe DY, Xia Y, Radially Aligned, Electrospun Nanofibers as Dural Substitutes for Wound Closure and Tissue Regeneration Applications, ACS Nano. 4, 2010, 5027.
[46] Li X, Li M, Sun J, Zhuang Y, Shi J, Guan D, *et al.*, Radially Aligned Electrospun Fibers with Continuous Gradient of SDF1α for the Guidance of Neural Stem Cells, Small. 12, 2016, 5009.
[47] Zhu Y, Cao Y, Pan J, Liu Y, Macro-alignment of electrospun fibers for vascular tissue engineering, J Biomed Mater Res Part B Appl Biomater. 92B, 2009, 508.
[48] Theron A, Zussman E, Yarin AL, Electrostatic field-assisted alignment of electrospun nanofibres, Nanotechnology. 12, 2001, 384.
[49] Zhou W, Li Z, Zhang Q, Liu Y, Wei F, Luo G, Gas Flow-Assisted Alignment of Super Long Electrospun Nanofibers, J Nanosci Nanotechnol. 7, 2007, 2667.
[50] Yang H, Kim S, Huh I, Kim S, Lahiji SF, Kim M, *et al.*, Rapid implantation of dissolving microneedles on an electrospun pillar array, Biomaterials. 64, 2015, 70.
[51] Pan C, Han Y, Dong L, Wang J, Gu Z, Electrospinning of Continuous, Large Area, Latticework Fiber onto Two-Dimensional Pin-array Collectors, J Macromol Sci Part B. 47, 2008, 735.
[52] Zheng G, Li W, Wang X, Wu D, Sun D, Lin L, Precision deposition of a nanofibre by near-field electrospinning, J Phys D Appl Phys. 43, 2010, 415501.
[53] Sharma CS, Katepalli H, Sharma A, Madou M, Fabrication and electrical conductivity of suspended carbon nanofiber arrays, Carbon N Y. 49, 2011, 1727.
[54] Chang T-L, Huang C-H, Chou S-Y, Tseng S-F, Lee Y-W, Direct fabrication of nanofiber scaffolds in pillar-based microfluidic device by using electrospinning and picosecond laser pulses, Microelectron Eng. 177, 2017, 52.
[55] RAWAT A, MAHAVAR HK, TANWAR A, SINGH PJ, Study of electrical properties of polyvinylpyrrolidone/polyacrylamide blend thin films, Bull Mater Sci. 37, 2014, 273.
[56] Qi X-Y, Yan D, Jiang Z, Cao Y-K, Yu Z-Z, Yavari F, *et al.*, Enhanced Electrical Conductivity in Polystyrene Nanocomposites at Ultra-Low Graphene Content, ACS Appl Mater Interfaces. 3, 2011, 3130.
[57] Ahmad A, Isa KBM, Osman Z, Conductivity and structural studies of plasticized polyacrylonitrile (PAN)-lithium triflate polymer electrolyte films, Sains Malaysiana. 40, 2011, 691.
[58] Collins G, Federici J, Imura Y, Catalani LH, Charge generation, charge transport, and residual charge in the electrospinning of polymers: A review of issues and complications, J Appl Phys. 111, 2012, 44701.

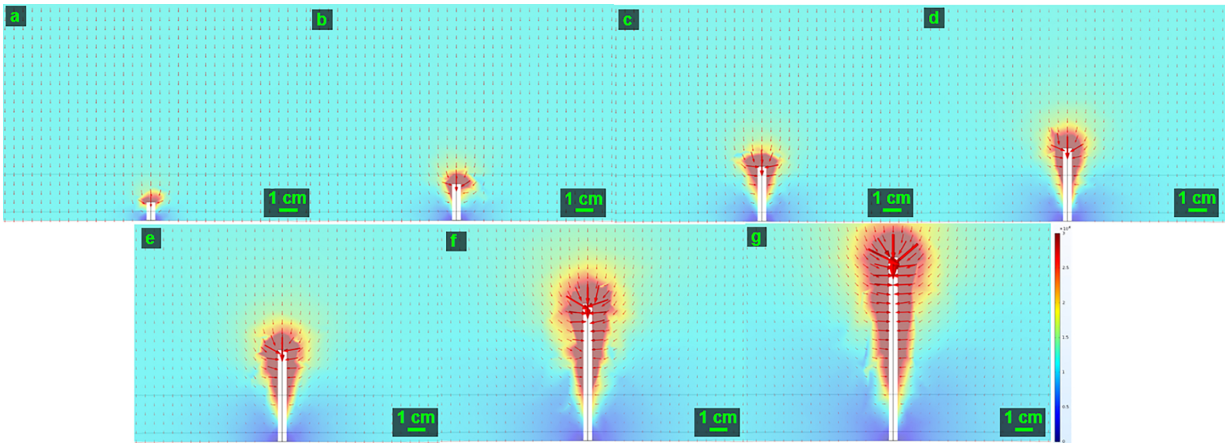

Figure S1: Electric field simulation in the vicinity of the grounded pillar. The height of the pillar alters the electric field lines close to the pillar. The electric field scale is in $V \cdot m^{-1}$.

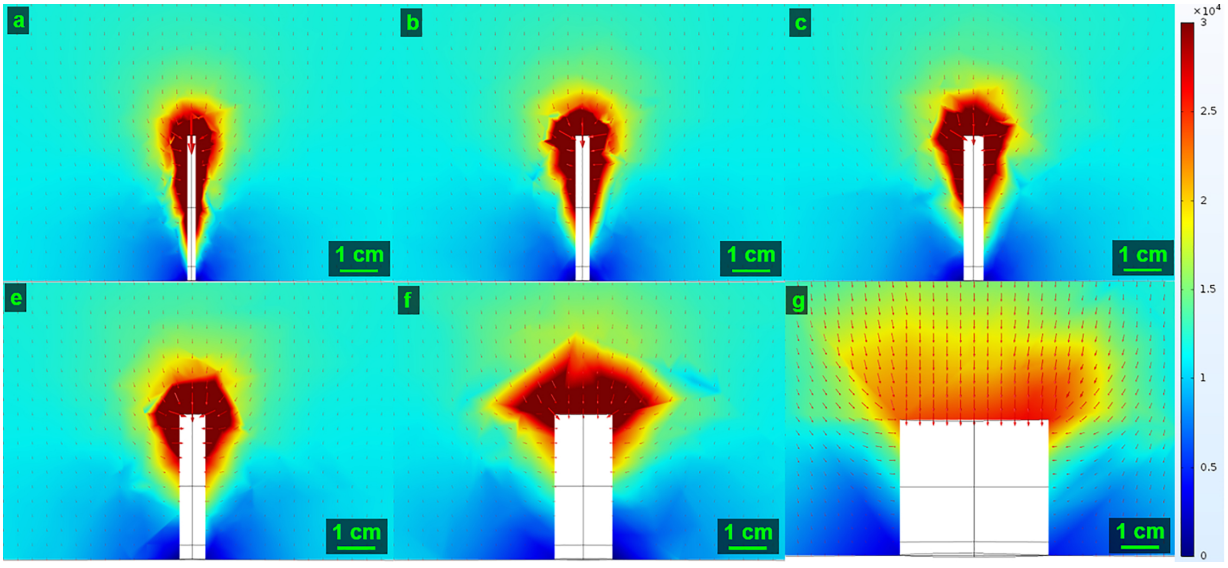

Figure S2: Electric field simulation in the vicinity of the grounded pillar. There is little to no change over the electric field lines on the sides of the pillar with increasing pillar thickness. The electric field scale is in $V \cdot m^{-1}$.

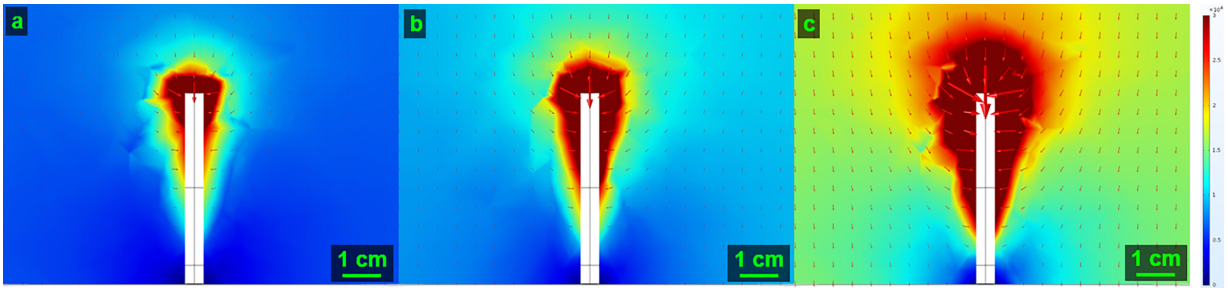

Figure S3: Evolution of the electric field with increasing voltage. Only the intensity of the electric field is altered because of the voltage, the direction stays roughly the same. The electric field scale is in $V \cdot m^{-1}$.

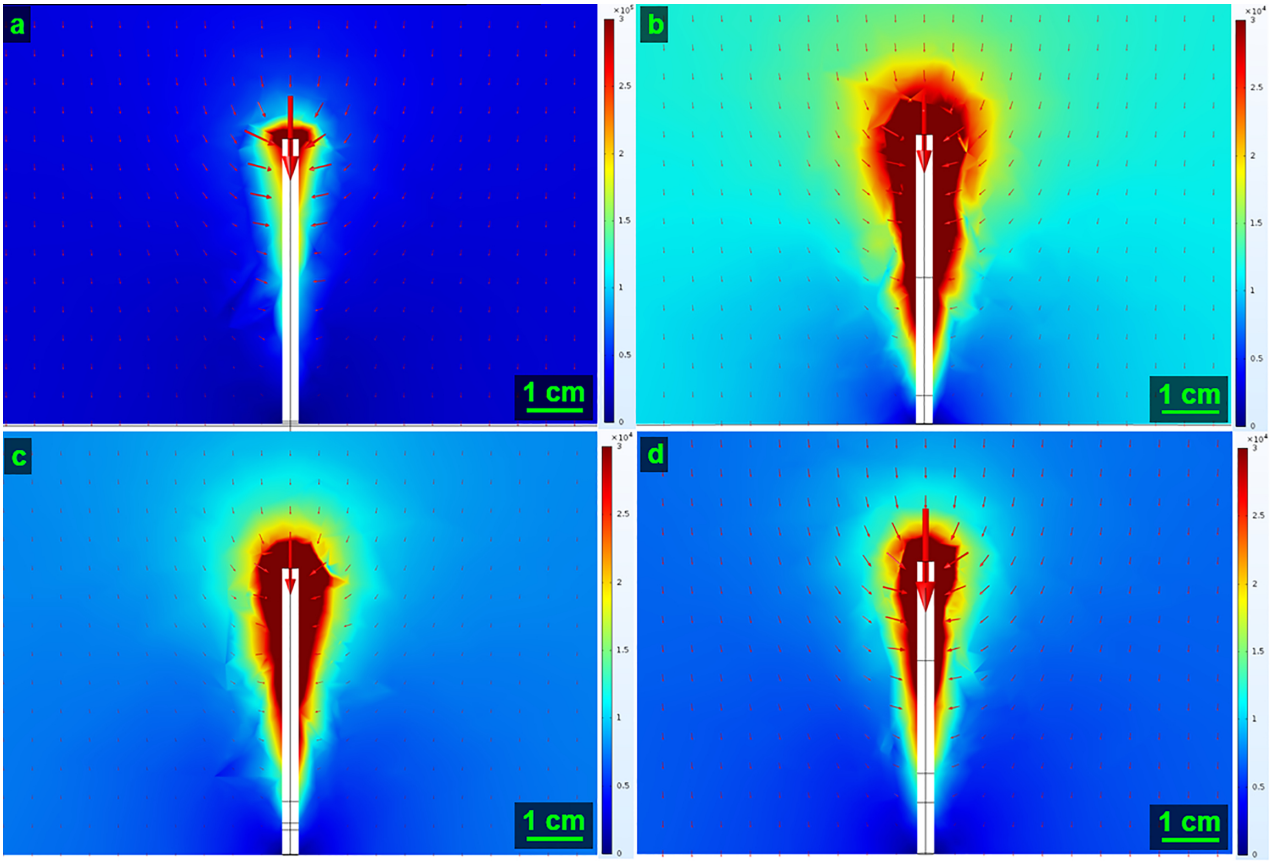

Figure S4: Evolution of the electric field with increasing working distance. The effect of increasing working distance on the electric field in the vicinity of the grounded pillar is similar to the effect of increasing voltage. The electric field scale is in $V \cdot m^{-1}$.

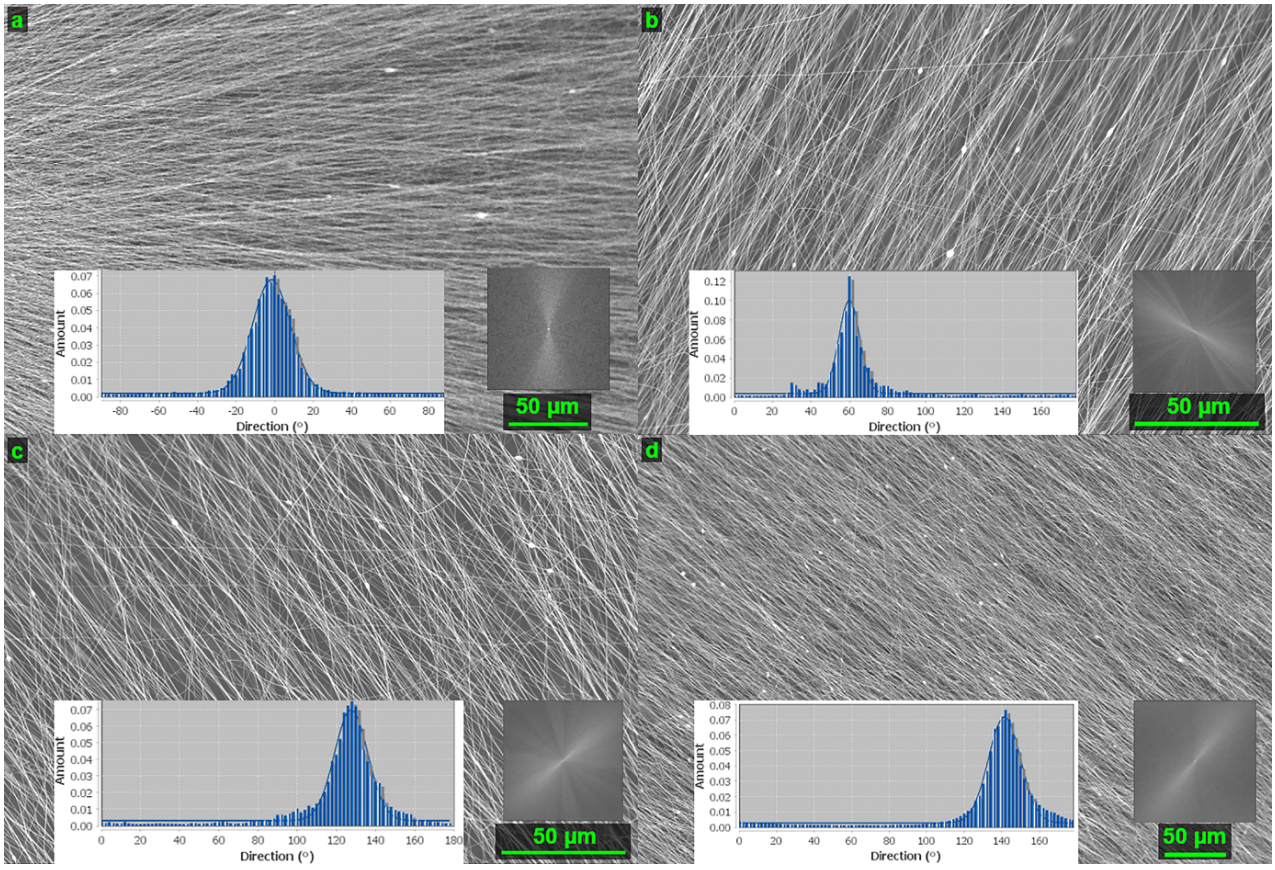

Figure S5: SEM picture of the fibers on the cone structure after electrospinning. The experimental conditions were the following: 15 wt% PVP/H_2O was electrospun at an applied voltage of +14 kV, a working distance of 10 cm and a flow rate of 0.25 mL·h^{-1}. The alignment of the fibers starting from the top of the cone is observable. The SEM pictures are associated with their Fast Fourier Transform and fibers orientation histogram. Different pillar morphology yields similar results. (a) Pillar height 0.7 mm and thickness 0.3 mm. (b) Pillar height 5 mm and thickness 0.3 mm. (c) Pillar height 5 mm and thickness 0.5 mm. (d) Pillar height 5 mm and thickness 2.0 mm.

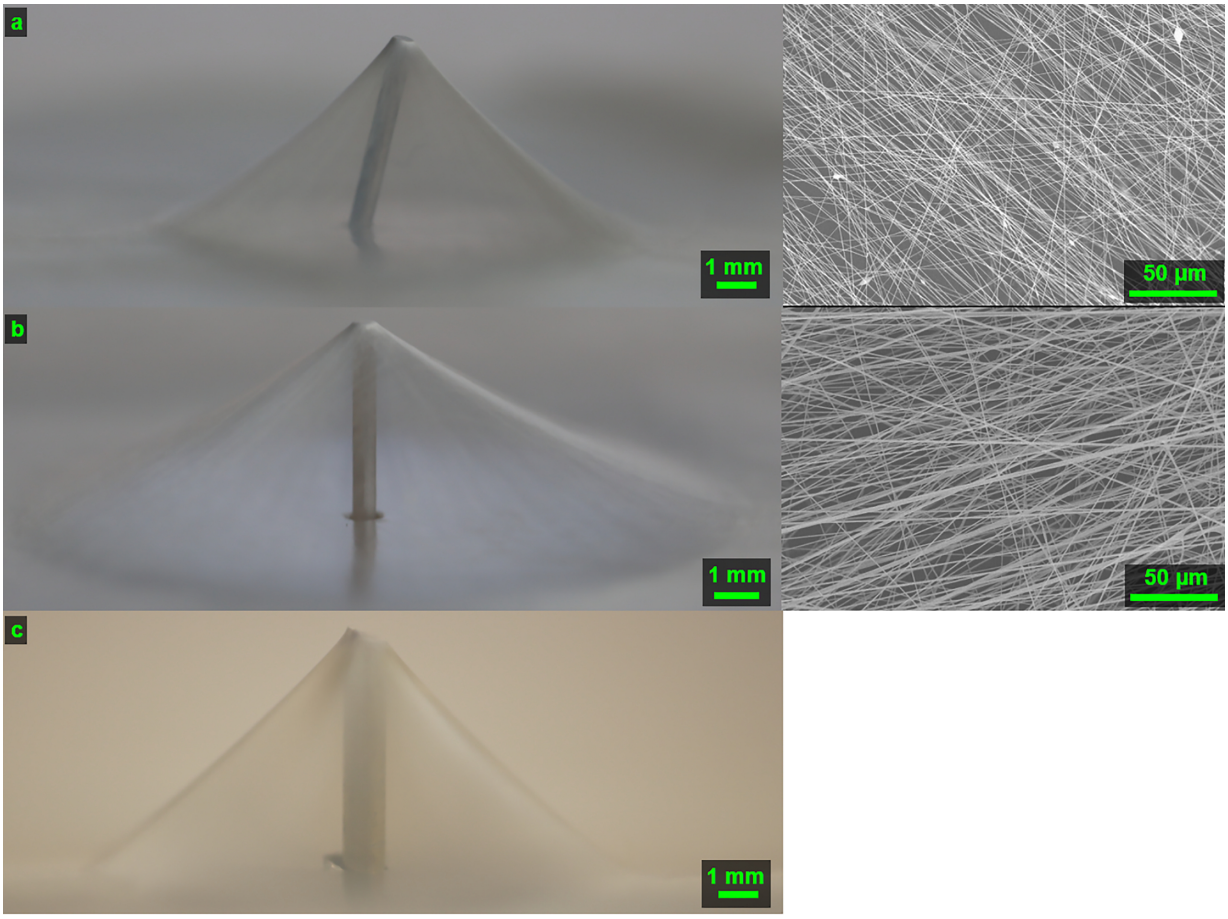

Figure S6: Macroscopic picture and SEM picture of other electrospun cone structures. a) 15 wt% PAN in DMF with standard graphite pillar. b) 15 wt% PS in 1:1 DMF/THF with standard graphite pillar. c) 15 wt% PVP in H_2O with steel/copper pillar.